

Differential flow correlations in relativistic heavy-ion collisions

Jing Qian^{1,*}, Ulrich Heinz², Ronghua He¹ and Lei Huo¹

¹ *Department of Physics, Harbin Institute of Technology,
Harbin, 150001, People's Republic of China and*

² *Department of Physics, The Ohio State University, Columbus, OH 43210-1117, USA**

(Dated: November 16, 2018)

Abstract

A systematic analysis of correlations between different orders of p_T -differential flow is presented, including mode coupling effects in flow vectors, correlations between flow angles (a.k.a. event-plane correlations), and correlations between flow magnitudes, all of which were previously studied with integrated flows. We find that the mode coupling effects among differential flows largely mirror those among the corresponding integrated flows, except at small transverse momenta where mode coupling contributions are small. For the fourth- and fifth-order flow vectors V_4 and V_5 we argue that the event plane correlations can be understood as the ratio between the mode coupling contributions to these flows and the flow magnitudes. We also find that for V_4 and V_5 the linear response contribution scales linearly with the corresponding cumulant-defined eccentricities but not with the standard eccentricities.

* Correspond to qianjing8758@gmail.com

I. INTRODUCTION

The ultimate goal of studying relativistic heavy ion collisions is to extract from experimentally measured final particle momentum distributions quantitatively precise information on the transport properties and dynamical evolution of the quark-gluon plasma (QGP) generated in these collisions. The azimuthal anisotropy of particle emission in the transverse plane, known as anisotropic flow, is one key observable suggesting that QGP behaves like an almost perfect liquid [1]. Using an azimuthal Fourier expansion of the single particle distribution up to harmonic order N , this anisotropy can be characterized by $2N$ parameters: the flow magnitude v_n and the flow angle Ψ_n relative to the reaction plane which is often called n -th order event plane angle ($1 \leq n \leq N$). They are combined into the complex flow vectors $V_n = v_n e^{in\Psi_n}$.

Due to quantum mechanical fluctuations in the initial conditions created in heavy-ion collisions, the flow vectors V_n fluctuate from event to event, even for identical impact parameters and collision systems. Correlations between anisotropic flow vectors of different orders have been studied both theoretically and experimentally. Examples are correlations between flow angles (a.k.a, event-plane correlations) [2–7], correlations between the magnitudes of the flow harmonics [8–10], and nonlinear mode coupling effects between flow vector contributing to V_n for $n > 3$ [11, 12]. These correlations may shed light on the fluctuating initial conditions, but their strength is also affected by dissipative effects on the dynamical evolution of the QGP.¹

Since measurements of such correlations are very statistics-hungry, existing correlation studies are almost exclusively for the integrated flows, using the flow vectors of all charged particles in a centrality rapidity window without differentiating them according to their transverse momentum. Given the continuously increasing number of collected data we here ask the question what would change if one performed this studies differentially in transverse momentum. We present a systematic study of the correlation between differential flows of different harmonic orders for Pb+Pb collisions at 2.76 TeV, using the VISH2+1 hydrodynamic code [13, 14] to describe the dynamical evolution of the collision. Admittedly, our study does not suffer from the same kind of statistical limitations faced by experimentalists: We use the Cooper-Frye prescription to compute the final particle spectra from the

¹ Even without E-b-E fluctuations, the even orders of flow are correlated because of the almond shaped deformation of the initial spatial distribution in noncentral collisions which is not of pure $\cos(2\phi)$ form.

hydrodynamic output, which yields a continuous final particle momentum distribution, corresponding to the limit of an infinite number of particles emitted from each event. Therefore, our results are affected only by fluctuations associated with the fluctuating initial conditions (which we sample by evolving 2000 events per centrality class through the hydrodynamic code) and not by finite number statistical fluctuations in the final state that arise in real experiments from the fact that Nature, due to the limited energy content of each event, can sample the final momentum distribution only with a finite number of particles. – We here use the MC-Glauber initial conditions as input, start the hydrodynamic evolution at $\tau_0 = 0.6 \text{ fm}/c$ without pre-equilibrium flow, and end it on an isothermal freeze-out surface of temperature $T_{\text{dec}} = 120 \text{ MeV}$. Unless otherwise stated, the shear viscosity is set to a default value of $\eta/s = 0.08$. Correlations between flow angles and flow magnitudes are discussed in Secs. II and III, respectively. In Sec. IV we present the mode coupling effects in higher order of differential flow vectors. The results are discussed and summarised in Sec. V. Some studies elucidating the meaning of the linear part (previously called the “linear response part”) of higher harmonic flows are presented in the Appendix.

II. CORRELATIONS BETWEEN FLOW ANGLES

Correlations between different flow angles are usually called event plane correlations whereas the correlations between the angles associated with the corresponding initial spatial eccentricities are known as participant plane correlations. These multi-plane correlations have yielded insight into the initial conditions and hydrodynamic evolution of heavy ion collisions [2–7].

To calculate the event plane correlations we use the scalar product definition which does not depend on the event-plane resolution [15]:

$$\langle \cos(c_1 n_1 \phi_{n_1} + \dots + c_k n_k \phi_{n_k}) \rangle \{ \text{SP} \} := \frac{\langle Q_{n_1}^{c_1} Q_{n_2}^{c_2} \dots Q_{n_k}^{c_k} \rangle}{\sqrt{\langle Q_{n_1}^{c_1} Q_{n_1}^{*c_1} \rangle \dots \langle Q_{n_k}^{c_k} Q_{n_k}^{*c_k} \rangle}}. \quad (1)$$

Here, $\langle \cos(4(\Psi_2 - \Psi_4)) \rangle \{ \text{SP} \}$ is chosen as an example of a two-plane correlation, and $\langle \cos(2\Psi_2 + 3\Psi_3 - 5\Psi_5) \rangle \{ \text{SP} \}$ as an example of a three-plane correlation:

$$\begin{aligned} \langle \cos(4(\Psi_2 - \Psi_4)) \rangle \{ \text{SP} \} &:= \frac{\langle V_4 V_2^{*2} \rangle}{\sqrt{\langle v_4^2 \rangle \langle v_2^4 \rangle}}, \\ \langle \cos(2\Psi_2 + 3\Psi_3 - 5\Psi_5) \rangle \{ \text{SP} \} &:= \frac{\langle V_5 V_2^* V_3^* \rangle}{\sqrt{\langle v_5^2 \rangle \langle v_2^2 \rangle \langle v_3^2 \rangle}}. \end{aligned} \quad (2)$$

From this definition we see that $\langle \cos(4(\Psi_2 - \Psi_4)) \rangle \{SP\}$ in fact equals the Pearson correlation coefficient between V_4 and V_2^2 . On the other hand, $\langle \cos(2\Psi_2 + 3\Psi_3 - 5\Psi_5) \rangle \{SP\}$ does not equal the Pearson correlation coefficient between V_5 and $V_2 V_3$ unless the fluctuations of the elliptic and triangular flows are uncorrelated and factorize as follows: $\langle v_2^2 v_3^2 \rangle = \langle v_2^2 \rangle \langle v_3^2 \rangle$. While this may be a reasonable assumption for v_2 and v_3 because v_3 is dominated by initial state fluctuations whereas v_2 has generally a strong geometric component, it is certainly not justifiable for the correlation between v_2^2 and v_4^2 which are correlated with each other by the deformed initial collision geometry in non-central collisions. This geometric correlation between the elliptic and quadrangular flow magnitudes affects the three-plane correlation $\langle \cos(2\Psi_2 + 4\Psi_4 - 6\Psi_6) \rangle \{SP\}$. This shows that event-plane correlations in general are not Pearson correlation coefficients between the corresponding V_n .

The event plane correlations (2) for differential (as a function of transverse momentum) and integrated flows are shown in Fig. 1 and compared with the corresponding participant plane correlations. Note that for the p_T -differential event plane correlators all correlated particles are taken from the same p_T bin. (This is different from the usual definition of second- or third-order p_T -differential flow cumulants (see e.g. [16]) where only one particle comes from the selected p_T bin and its flow vector is correlated with others constructed from all charged hadrons.) Red circles denote event-plane correlations of differential flows from ideal hydrodynamic evolution, and the red shaded bands show the corresponding p_T -integrated event-plane correlations of integrated for the same events for comparison. Blue triangles and blue shaded bands show the analogous correlations for events that were evolved with viscous hydrodynamics using shear viscosity $\eta/s = 0.08$. The upper (lower) panels are for central (0-5% centrality) and mid-peripheral (40-50% centrality) collisions.

Similar to what was observed for the p_T -integrated flows, the event plane correlations between the p_T -differential flows increase with impact parameter from central to semi-peripheral collisions. Shear viscosity increases the strength of the event-plane correlation as previously found by Yan [3] and Qiu [7] for p_T -integrated flows. The shear viscous strengthening of the correlations is relatively more pronounced in central than in more peripheral collisions, but it appears to disappear at higher p_T values. At low p_T , the differential event plane correlations are much weaker than those of the integrated flows and almost negligible. Increasing with p_T , the differential event plane correlations become approximately equal to those of the integrated flows around $p_T \approx 0.5$ GeV/ c ; at even larger p_T , however, for viscous

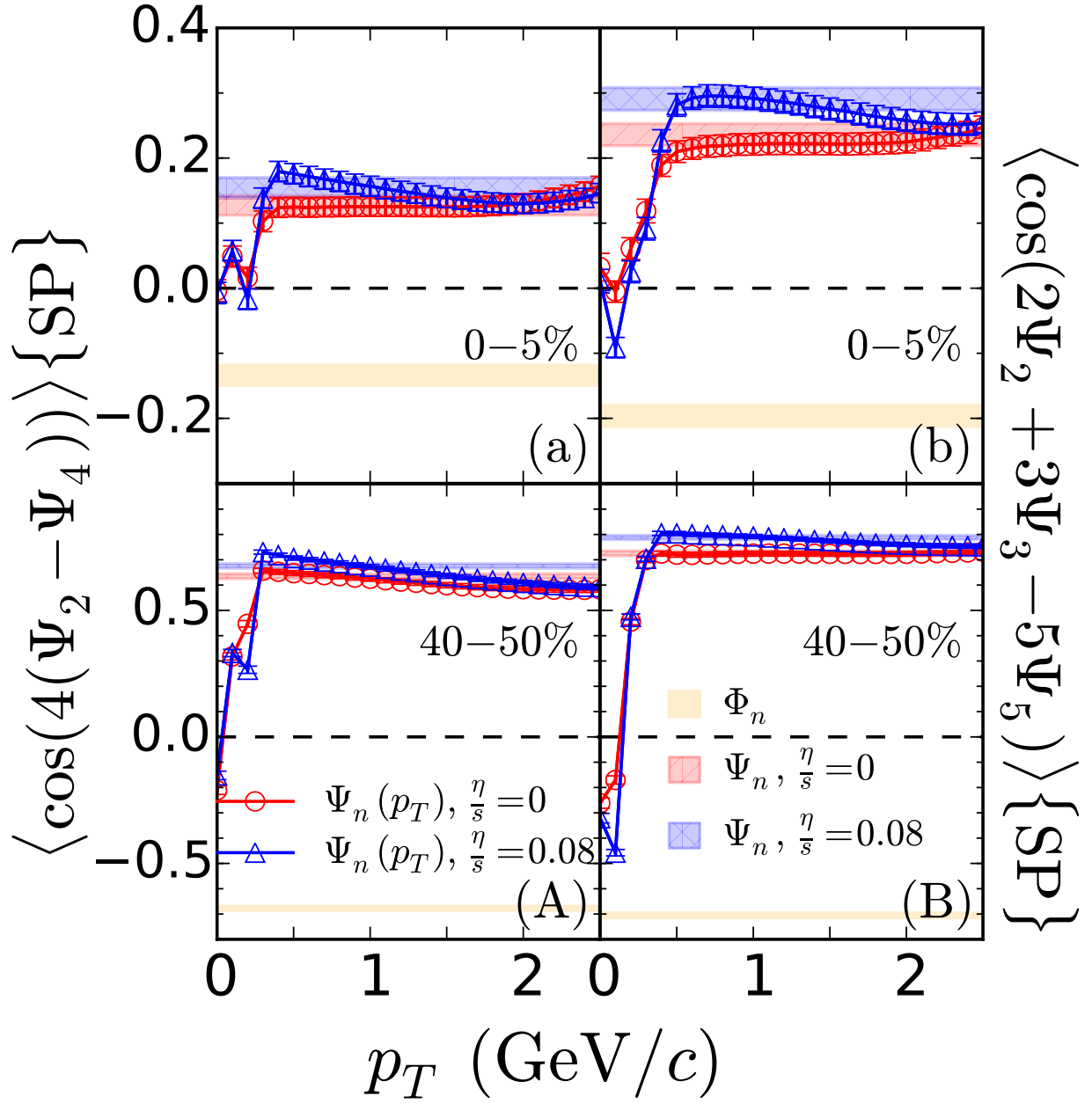


FIG. 1. (Color online) p_T dependence of the two- and three-plane correlations $\langle \cos(4(\Psi_2 - \Psi_4)) \rangle \{SP\}$ and three-plane correlation $\langle \cos(2\Psi_2 + 3\Psi_3 - 5\Psi_5) \rangle \{SP\}$. Subgraphs (a-b) are for events of 0-5% centrality while (A-B) are for 40-50% centrality. In each centrality class 2000 hydrodynamic events are used for the analysis. Red and blue represent ideal and viscous hydrodynamic results, respectively. Markers show event-plane correlations for differential flows, and colored bands are those for the corresponding integrated flows shown for comparison. The corresponding participant plane correlations are shown as yellow bands. The widths of the bands indicate the corresponding variances due to event-by-event fluctuations.

evolution the p_T -differential correlations drop below the p_T -integrated values, indicating that the viscous strengthening of the event-plane correlations operates only at thermal transverse

momenta and disappears for harder p_T .

The differences between differential and integrated event plane correlations can to a large extent be explained as a consequence of the decorrelation between the flow angles at different p_T -values. As noted in [17], in general the flow angle Ψ_n depend on p_T and, as a function of p_T , $\Psi_n(p_T)$ wanders around the ‘average angle’ Ψ_n . The p_T -averaged event-plane correlator thus closely represents the p_T -differential one only in the p_T -region in which the majority of particles are emitted. At small p_T , the variance $\sigma(\Psi_n(p_T) - \Psi_n)$ is quite large for all n due to the fluctuating $\Psi_n(p_T)$. This is the likely reason for the much weaker event-plane correlations of the p_T -differential flows at small p_T compared to the p_T -averaged ones: At small p_T , the directions of the complex flow vectors are almost uncorrelated [18]. For this reason, we will mostly ignore the low- p_T region in the rest of the paper.

III. CORRELATIONS BETWEEN FLOW MAGNITUDES

There are mainly two ways to describe the correlations between flow magnitudes: One way is to study the correlation between v_m and v_n via the event-shape selection method, suggested by the ATLAS collaboration [8, 19] and already tested with the hydrodynamic model [9]. The other way is using the Symmetric 2-harmonic 4-particle Cumulant (or Moment) $SC(m, n)$ to evaluate the correlation between v_m and v_n , suggested by the ALICE Collaboration [10] and tested with hydrodynamic, transport and hybrid models. In particular, the authors of [20] studied the p_T dependence of the normalized correlators $SC(m, n)$, ie. $NSC^v(m, n) \equiv \frac{\langle v_m^2 v_n^2 \rangle - \langle v_m^2 \rangle \langle v_n^2 \rangle}{\langle v_m^2 \rangle \langle v_n^2 \rangle}$, between the magnitudes of the differential flows $v_m(p_T)$ and $v_n(p_T)$ at 20-30% centrality with the VISH2+1 and AMPT models. They found that for both models, $NSC^v(3, 2)$ and $NSC^v(4, 3)$ change sign from negative to positive with increasing p_T around at $p_T \sim 3 \text{ GeV}/c$.

Furthermore, Niemi and collaborators studied the linear correlation coefficient $c(v_m, v_n)$ of the differential flows $v_m(p_T)$ and $v_n(p_T)$ as a function of transverse momentum for 20-30% Au+Au collisions at $\sqrt{s_{\text{NN}}} = 200 \text{ GeV}$ with the hydrodynamic model [21]. In their calculation, $c(v_2, v_3)$ and $c(v_3, v_4)$ also exhibit a sign change with increasing p_T . However, they argued that at 20-30% centrality, (v_2, v_3) and (v_3, v_4) are not linearly correlated since $c(v_2, v_3) \approx c(v_3, v_4) \approx 0$. They also suggested that the differential $c(v_2, v_4)(p_T)$ is sensitive to shear viscosity and decoupling temperature and is strongly affected by $c(\epsilon_2, \epsilon_4)$ in the

initial state.

In this paper, we use the event-shape selection method to study the correlations between differential flows [19]. Building on previous work reported in [9], 42000 hydrodynamically generated events were divided into 14 equal centrality classes according to multiplicity, then ordered by q_n and subdivided by percentile into 6 bins per centrality class (0–0.1, 0.1–0.2, 0.2–0.5, 0.5–0.8, 0.8–0.9, and 0.9–1.0) where $\mathbf{q}_n = q_n e^{in\Psi_n^q} \equiv \langle m_T e^{in\phi_p} \rangle / \langle m_T \rangle$ (with $m_T = \sqrt{m^2 + p_T^2}$). The differential flow magnitude is calculated as $v_n\{2\}(p_T) = \langle v_n(p_T) v_n \cos(n(\Psi_n(p_T) - \Psi_n)) \rangle / \sqrt{\langle v_n^2 \rangle}$; here v_n is n -th order integrated flow coefficient and $\langle \dots \rangle$ denotes the average over events in one q_2 (or q_3) bin.

Before discussing the correlations between the differential flow magnitudes further we would like to emphasize that the event shape selection based on q_n yields equivalent event classes for different p_T ranges. As seen in Fig. 6 in [8] for $n = 2$ and 3, v_n for the range $0.5 < p_T < 2$ GeV shows approximate linearity with v_n in the range $3 < p_T < 4$ GeV, for different q_n bins and in all centrality classes.

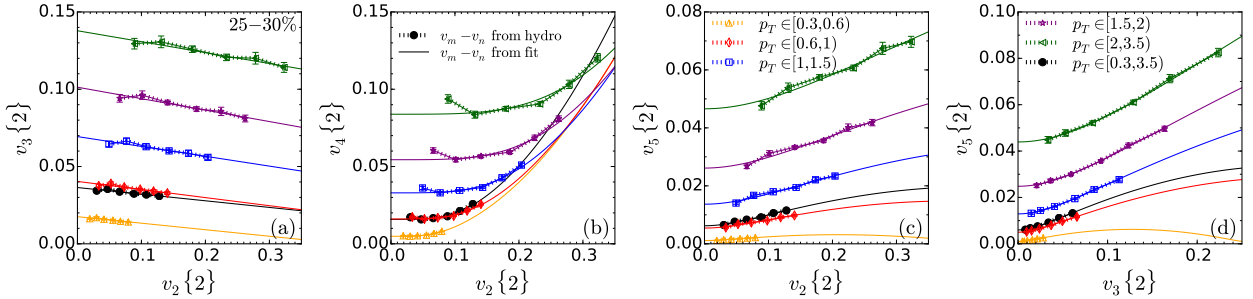


FIG. 2. (Color online) $v_m\{2\}$ vs. $v_n\{2\}$ for different p_T ranges at 25-30% centrality, calculated with viscous hydrodynamics using $\eta/s = 0.08$. 3000 events in each 5% centrality bin are used for the analysis. While solid black circles represent the integrated $v_m\{2\} - v_n\{2\}$ correlations, the colored hollow markers show the correlations at different p_T . Markers connected by dotted lines represent the hydrodynamic results; the solid lines are fits using Eqs. (3).

Fig. 2 shows the correlations between v_m and v_n for different p_T ranges, at 25-30% collision centrality. Differently colored lines represent flows calculated within different p_T ranges while different points along a line of given color represent different q_n bins (q_2 bins for the left three panels, q_3 bins for the right panel). The solid black circles connected by dotted lines are the p_T -integrated $v_m - v_n$ correlations for comparison.

Since the differential v_m and v_n all increase with p_T in the p_T ranges shown here, and the integrated flows are the yield-weighted averages of the differential flows, the p_T -integrated

black lines are in the middle of the colored lines representing p_T -differential correlations. In fact, the p_T -integrated $v_m - v_n$ correlation is quite close to the differential one for the range $0.6 < p_T < 1$ GeV/ c . As for the p_T -integrated flows [8, 9], the differential v_4 and v_5 are positively correlated with the differential v_2 whereas v_3 is anticorrelated with v_2 . In Ref. [9] the following fit functions were found to yield good representations of the p_T -integrated $v_m - v_n$ correlations:

$$\begin{aligned} v_3\{2\} &= v_3^0 + k_3 v_2\{2\}, \\ v_4\{2\} &= \sqrt{(v_4^0)^2 + (k_4 v_2\{2\})^2}, \\ v_5\{2\} &= \sqrt{(v_5^0)^2 + (k_5 v_2\{2\} v_3\{2\})^2}. \end{aligned} \tag{3}$$

The solid colored lines in Fig. 2 show that these fit functions represent the p_T -differential correlations equally well. The corresponding fit parameters are plotted as functions of centrality in Fig. 3, v_n^0 in the left and k_n in the right panels. One sees that the fit parameters for the differential flow correlations at different p_T have similar centrality dependences as those for the integrated flows. Except for the most central collisions, k_n decreases with impact parameter. k_3 is negative, due to the anti-correlation between v_3 and v_2 except for the most central collisions. As discussed in [9] the latter is caused by neglecting p - p multiplicity fluctuations in the initial conditions used in this study. k_4 and k_5 are both positive. Using q_2 or q_3 in the event-shape selection leads to some differences in the fitted parameters for v_5 . The new information from the p_T -differential analysis is that v_n^0 increases while k_n decreases with increasing p_T , for all n . This means that, as p_T increases, the linear contribution $v_n^0(p_T)$ increases in sync with $v_n(p_T)$ whereas the strength of the non-linear mode coupling described by $k_n(p_T)$ decreases. Another interesting observation is that k_4 and k_5 of the p_T -integrated flows are larger than those of the p_T -differential flows, in all p_T ranges and at all collision centralities. We will discuss this further in the next section.

IV. MODE COUPLING EFFECTS IN THE DIFFERENTIAL FLOW VECTORS

It has now been established that, while V_2 and V_3 respond almost linearly to their corresponding initial eccentricity vectors, V_4 and higher harmonic flows are affected by significant nonlinearities in their response. In [11, 12], V_n ($n > 3$) was decomposed into linear response

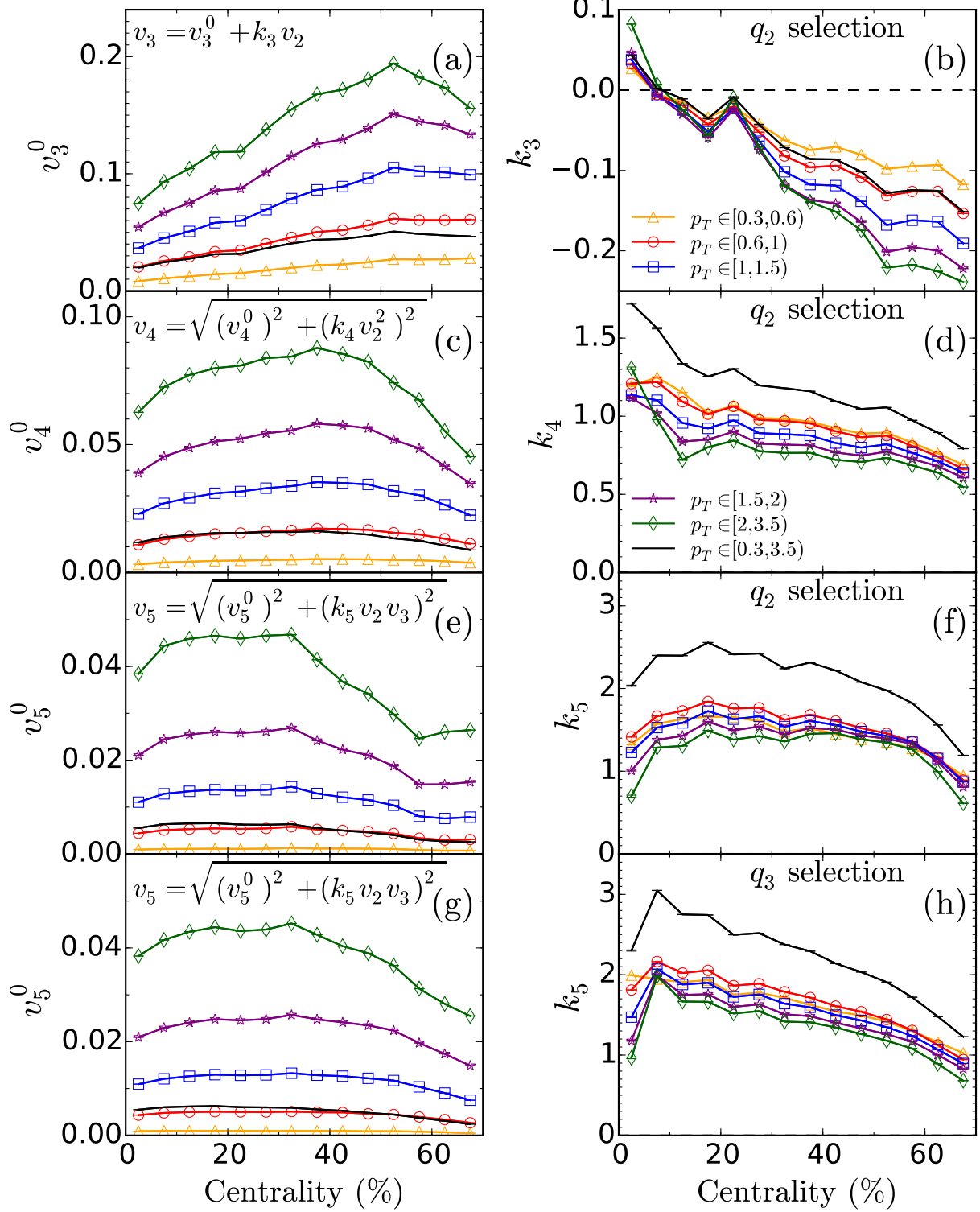


FIG. 3. (Color online) Centrality dependence of the parameters v_n^0 and k_n extracted from the fits of the $v_m\{2\} - v_n\{2\}$ correlations shown in Fig. 2 with Eqs. (3), for the different p_T ranges (colored markers)) as well as the p_T -averaged correlation (black lines) shown in that figure, using the same color coding.

and nonlinear mode coupling contributions as follows:

$$\begin{aligned}
V_4 &= V_{4L} + \chi_{422} V_2^2, \\
V_5 &= V_{5L} + \chi_{523} V_2 V_3, \\
V_6 &= V_{6L} + \chi_{624} V_2 V_{4L} + \chi_{633} V_3^2 + \chi_{6222} V_2^3, \\
V_7 &= V_{7L} + \chi_{725} V_2 V_{5L} + \chi_{734} V_3 V_{4L} + \chi_{7223} V_2^2 V_3.
\end{aligned} \tag{4}$$

Some questions about the interpretation of V_{nL} as the linear response contribution to the corresponding initial eccentricity were raised in Ref. [12]. In the Appendix we contribute to the further clarification of this question by showing empirically that for $n = 4$ and 5 V_{nL} responds approximately linearly to the cumulant-based but not to the moment-based initial eccentricities, as first suggested in [22, 23]. The mode coupling coefficients in Eqs. (4) are defined by

$$\begin{aligned}
\chi_{422} &= \frac{\text{Re}\langle V_4(V_2^*)^2 \rangle}{\langle v_2^4 \rangle}, \quad \chi_{523} = \frac{\text{Re}\langle V_5 V_2^* V_3^* \rangle}{\langle v_2^2 v_3^2 \rangle}, \\
\chi_{624} &= \text{Re} \frac{\langle V_6 V_2^* V_4^* \rangle \langle v_2^4 \rangle - \langle V_6 V_2^{*3} \rangle \langle V_4 V_2^{*2} \rangle}{(\langle v_4^2 \rangle \langle v_2^4 \rangle - \langle V_4 V_2^{*2} \rangle^2) \langle v_2^2 \rangle}, \\
\chi_{633} &= \frac{\text{Re}\langle V_6 V_3^{*2} \rangle}{\langle v_3^4 \rangle}, \quad \chi_{6222} = \frac{\text{Re}\langle V_6 V_2^{*3} \rangle}{\langle v_2^6 \rangle}, \\
\chi_{725} &= \text{Re} \frac{\langle V_7 V_2^* V_5^* \rangle \langle v_2^2 v_3^2 \rangle - \langle V_7 V_2^{*2} V_3^* \rangle \langle V_5 V_2^* V_3^* \rangle}{(\langle v_5^2 \rangle \langle v_2^2 v_3^2 \rangle - \langle V_5 V_2^* V_3^* \rangle^2) \langle v_2^2 \rangle}, \\
\chi_{734} &= \text{Re} \frac{\langle V_7 V_3^* V_4^* \rangle \langle v_2^4 \rangle - \langle V_7 V_2^{*2} V_3^* \rangle \langle V_4 V_2^{*2} \rangle}{(\langle v_4^2 \rangle \langle v_2^4 \rangle - \langle V_4 V_2^{*2} \rangle^2) \langle v_3^2 \rangle}, \\
\chi_{7223} &= \frac{\text{Re}\langle V_7 V_2^{*2} V_3^* \rangle}{\langle v_2^4 v_3^2 \rangle}.
\end{aligned} \tag{5}$$

As discussed in the preceding section, the p_T -differential flows exhibit qualitatively similar mode coupling effects as the integrated flows. To quantify them we compute the mode coupling coefficients for the differential flows according to Eqs. (5) and show their p_T dependence in Fig. 4. The p_T -differential mode coupling coefficients show similar centrality dependence as the integrated ones (shown as colored shaded bands) and generally have only a weak dependence on p_T , except at small p_T . The strong variation of the mode coupling coefficients at small p_T is related to the similarly strong p_T -dependence of the event-plane correlators shown in Fig. 1 and can again be attributed to the large variance of the flow angles Ψ_n at small p_T .

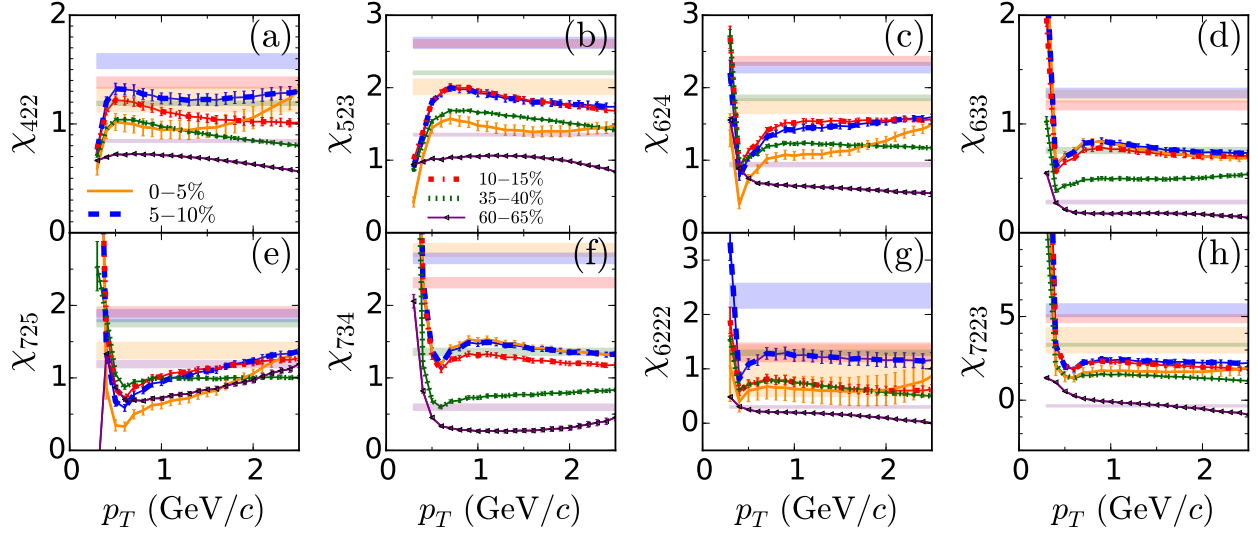


FIG. 4. (Color online) p_T dependence of the mode coupling coefficients for p_T -differential flows from viscous hydrodynamics with $\eta/s = 0.08$. Lines of different colors and styles represent different collision centralities. Each 5% centrality bin contains 3000 events. For comparison, shaded bands of the same color as the lines show the mode coupling coefficients for the integrated flows corresponding to the same centrality.

In the p_T regions where p_T -differential mode coupling coefficients show only weak p_T dependence their magnitudes are generically smaller than those of the integrated flows, for almost all modes and for all collision centralities studied here. To understand this intuitively let us consider the case of quadrangular flow in the approximation where the non-linear mode coupling contribution dominates:

$$\begin{aligned}
 V_4 &\approx \chi_{422} V_2^2, & V_4(p_T) &\approx \chi_{422}(p_T) V_2^2(p_T), \\
 \chi_{422} &\approx \frac{V_4}{V_2^2} = \frac{v_4 e^{i4\Psi_4}}{v_2^2 e^{i4\Psi_2}} = \frac{v_4}{v_2^2} \\
 &= \frac{\{v_4(p_T)\}}{\{v_2(p_T)\}^2} = \frac{\{\chi_{422}(p_T) v_2^2(p_T)\}}{\{v_2(p_T)\}^2}
 \end{aligned} \tag{6}$$

Here $\{\dots\}$ denotes symbolically the averaging of the differential flow over p_T . If $\chi_{422}(p_T)$ is independent of p_T (which according to Fig. 4 is approximately true for $p_T \geq 0.5$ GeV/c) then

$$\chi_{422} \approx \chi_{422}(p_T) \frac{\{v_2^2(p_T)\}}{\{v_2(p_T)\}^2} \geq \chi_{422}(p_T). \tag{7}$$

As observed above when discussing the $v_m - v_n$ correlations, the k_n values associated with the integrated flows are also larger than those of the p_T -differential flows. In fact, both the χ and k coefficients describe mode coupling effects, and hence they are tightly connected.

Taking $n = 4$ as an example, this is illustrated by combining Eqs. (3) and (4) as follows:

$$\begin{aligned}\langle v_4^2 \rangle &= (v_4^0)^2 + k_4^2 \langle v_2^2 \rangle^2 \\ &= \langle v_{4L}^2 \rangle + \chi_{422}^2 \langle v_2^4 \rangle = \langle v_{4L}^2 \rangle + \chi_{422}^2 \left(\langle v_2^2 \rangle^2 + \sigma_{v_2^2}^2 \right).\end{aligned}\quad (8)$$

Here $\sigma_{v_2^2}^2$ is the variance of v_2^2 , and we used $\langle V_{4L} V_2^{*2} \rangle \approx 0$ [11, 12]. Using the first of these equations, a similar argument as in Eqs. (6,7) provides support for our observation that $k_4 \geq k_4(p_T)$.

Using the decomposition (4) for the higher-order flows in the form $\langle v_n^2 \rangle = v_{nL}^2 + v_{nM}^2$ we can separate the linear and mode coupling terms as follows:

$$\begin{aligned}v_{4L} &= \sqrt{\langle v_4^2 \rangle - \frac{|\text{Re}\langle V_4 V_2^{*2} \rangle|^2}{\langle v_2^4 \rangle}}, & v_{4M} &= \frac{|\text{Re}\langle V_4 V_2^{*2} \rangle|}{\sqrt{\langle v_2^4 \rangle}}, \\ v_{5L} &= \sqrt{\langle v_5^2 \rangle - \frac{|\text{Re}\langle V_5 V_2^* V_3^* \rangle|^2}{\langle v_2^2 v_3^2 \rangle}}, & v_{5M} &= \frac{|\text{Re}\langle V_5 V_2^* V_3^* \rangle|}{\sqrt{\langle v_2^2 v_3^2 \rangle}}.\end{aligned}\quad (9)$$

Figure 5 shows the linear and mode-coupling contributions to the p_T -differential flows, v_{nL} and v_{nM} as defined in Eqs. (9), together with the ratio of the latter with $v_{n,\text{rms}}(p_T) \equiv \sqrt{\langle v_n^2(p_T) \rangle}$ (which indicates the relative importance of the mode-coupling terms to the p_T -differential flows), as functions of p_T for different collision centralities. Similar to what was observed earlier for the p_T -integrated flows [12], the linear and mode-coupling contributions to the differential flows exhibit opposite centrality dependences: the linear terms depend relatively weakly on centrality whereas the mode-coupling terms increase rapidly with increasing impact parameter.

Comparing the definition (1) of the event plane correlations with Eqs. (9) for the mode-coupling contributions v_{nM} one sees that for $n = 4, 5$ the correlation of the n th order event plane with those of lower harmonic order is, in fact, given by the fraction $v_{nM}/v_{n,\text{rms}}$ of the n th order rms flow $v_{n,\text{rms}}$ contributed by mode-coupling effects, plotted in the bottom row of Fig. 5.²

$$\begin{aligned}\langle \cos(4(\Psi_2 - \Psi_4)) \rangle \{ \text{SP} \} &= \frac{\langle V_4 V_2^{*2} \rangle}{\sqrt{\langle v_4^2 \rangle \langle v_2^4 \rangle}} = \frac{v_{4M}}{v_{4,\text{rms}}}, \\ \langle \cos(2\Psi_2 + 3\Psi_3 - 5\Psi_5) \rangle \{ \text{SP} \} &= \frac{\langle V_5 V_2^* V_3^* \rangle}{\sqrt{\langle v_5^2 \rangle \langle v_2^2 \rangle \langle v_3^2 \rangle}} = \frac{v_{5M}}{v_{5,\text{rms}}}.\end{aligned}\quad (10)$$

² More precisely, the two observables are equal up to a sign. For example, $\langle \cos(4(\Psi_2 - \Psi_4)) \rangle \{ \text{SP} \} = \text{sign}(\chi_{422}) v_{4M}/v_{4,\text{rms}}$. Since the two event plane correlators discussed in this paper, $\langle \cos(4(\Psi_2 - \Psi_4)) \rangle \{ \text{SP} \}$ and $\langle \cos(2\Psi_2 + 3\Psi_3 - 5\Psi_5) \rangle \{ \text{SP} \}$, are mostly positive (except at small p_T where the event planes fluctuate strongly) we omit the sign for short.

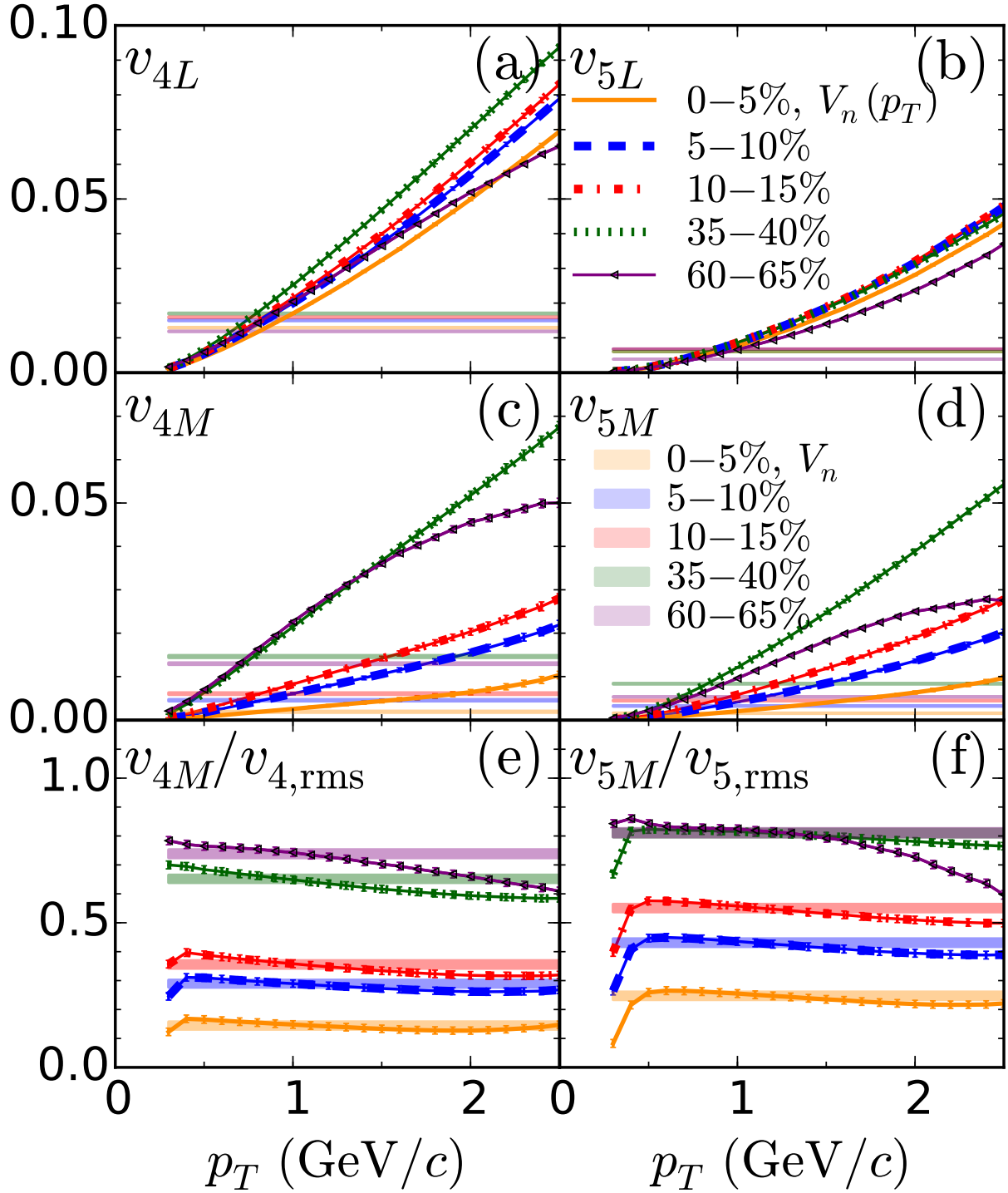


FIG. 5. (Color online) p_T dependence of v_{nL} , v_{nM} and $v_{nM}/v_{n,rms}$ for $n = 4, 5$ from viscous hydrodynamics with $\eta/s = 0.08$. Lines with different colors and symbols represent different centrality classes, with 3000 events in each 5% centrality bin. For comparison, the colored shaded bands show the corresponding values for the p_T -integrated flows.

That means that for $n = 4, 5$ the mode coupling contributions to the flow magnitudes are

caused by correlations between the n th-order and lower-order event planes. By implication, the smallness of the event plane correlations shown in Fig. 1 near $p_T = 0$ should lead to similarly small mode coupling contributions to $v_{4,5}(p_T)$ at small p_T . While this p_T region is not shown in Fig. 5, for reasons explained in Sec. II, the bottom panels in Fig. 5 indicate a steep drop of the mode coupling contributions to v_4 and v_5 below $p_T \sim 0.5 \text{ GeV}/c$. At higher p_T , the approximate p_T -independence of the event plane correlations shown in Fig. 1 is reflected in the flatness of $v_{nM}(p_T)/v_{n,\text{rms}}(p_T)$ shown in the bottom panels of Fig. 5.

Since, except for small p_T , the differential flows $v_{4,5}(p_T)$ receive a mode-coupling contribution that is almost independent of p_T , the mode-coupling contribution to their p_T -integrated analogues is very similar. The shaded bands in Figs. 5e,f show this. The above connection between mode-coupling effects and event plane correlations thus provides an explanation for the similarity of the strengths of the event plane correlations for p_T -integrated and p_T -differential flows noted in the discussion of Fig. 1 in Sec. II.

V. SUMMARY AND CONCLUSIONS

Using viscous hydrodynamics as a model for the dynamical evolution of Pb-Pb collisions at the LHC we presented a first systematic study of the correlations between different harmonic orders of the p_T -differential anisotropic flows of charged hadrons. We identified nonlinear mode coupling contributions to the differential flow, studied their p_T and centrality dependence and compared them with those for the p_T -integrated flows. We identified correlations with lower-order event planes as the main contributor to the mode coupling effects seen in the magnitudes of higher-order harmonic flows. Except for very low p_T , the mode coupling fraction depends very weakly on transverse momentum, and this is reflected in event plane correlations between the differential flows that are close to those of the integrated flows and largely independent of p_T . At very low p_T they exhibit strong p_T dependence, caused by large, p_T -dependent fluctuations of the flow angle. These event plane fluctuations destroy the mode coupling contributions to the higher-order flow magnitudes at low p_T , by averaging them away. Correlations between the magnitudes of the p_T -differential flows of different order have similar strength and centrality dependence as those between the corresponding integrated flows. The mode-coupling coefficients extracted from a two-component fit using event-shape engineering techniques were found to be smaller for the

p_T -differential flows than those for the integrated flows. This observation has a simple explanation as described in Sec. IV. The linear part of the two-component fit was shown to reflect the linear hydrodynamic flow response to the cumulant-based initial eccentricities but not to their standard moment-based analogues.

ACKNOWLEDGMENTS

The authors thank Jia Liu, Christopher Plumberg and Jianyi Chen for discussions. The research of UH was supported by the U.S. Department of Energy, Office of Science, Office for Nuclear Physics under Award DE-SC0004286. Computing resources were generously provided by the Ohio Supercomputer Center [25].

Appendix A: Discussion of V_{nL}

Usually, the eccentricities of the initial spatial distributions of energy or entropy are defined as moments with weight r^n : $\mathcal{E}_n = \epsilon_n e^{in\Phi_n} \equiv -\frac{\langle r^n e^{in\phi} \rangle}{\langle r^n \rangle}$ (for $n > 1$). The authors of [22, 23] suggested a different set \mathcal{E}'_n of eccentricity coefficients using spatial cumulants:

$$\begin{aligned}
\mathcal{E}'_2 &\equiv \epsilon_2 e^{i2\Phi_2} = \mathcal{E}_2, & \mathcal{E}'_3 &\equiv \epsilon_3 e^{i3\Phi_3} = \mathcal{E}_3, \\
\mathcal{E}'_4 &\equiv \epsilon'_4 e^{i4\Phi'_4} \equiv -\frac{\langle z^4 \rangle - 3\langle z^2 \rangle^2}{\langle r^4 \rangle} = \mathcal{E}_4 + \frac{3\langle r^2 \rangle^2}{\langle r^4 \rangle} \mathcal{E}_2^2, \\
\mathcal{E}'_5 &\equiv \epsilon'_5 e^{i5\Phi'_5} \equiv -\frac{\langle z^5 \rangle - 10\langle z^2 \rangle \langle z^3 \rangle}{\langle r^5 \rangle} = \mathcal{E}_5 + \frac{10\langle r^2 \rangle \langle r^3 \rangle}{\langle r^5 \rangle} \mathcal{E}_2 \mathcal{E}_3, \\
\mathcal{E}'_6 &\equiv \epsilon'_6 e^{i6\Phi'_6} \equiv -\frac{\langle z^6 \rangle - 15\langle z^2 \rangle \langle z^4 \rangle - 10\langle z^3 \rangle^2 + 30\langle z^2 \rangle^3}{\langle r^6 \rangle} \\
&= \mathcal{E}_6 + \frac{15\langle r^2 \rangle \langle r^4 \rangle}{\langle r^6 \rangle} \mathcal{E}_2 \mathcal{E}_4 + \frac{10\langle r^3 \rangle^2}{\langle r^6 \rangle} \mathcal{E}_3^2 + \frac{30\langle r^2 \rangle^3}{\langle r^6 \rangle} \mathcal{E}_2^3.
\end{aligned} \tag{A1}$$

Here $z \equiv x + iy = r e^{i\phi}$. Note that \mathcal{E}_1 (which is not used in our discussion) has a different definition.

By defining eccentricities using cumulants instead of moments one subtracts contributions from lower order z correlations. This led Teaney and Yan to suggest [22, 23] that the linear hydrodynamic response contribution to higher order flows should be linearly proportional to the cumulant-defined eccentricities and not to the traditional moment-defined ones. They also used this hypothesis to successfully explain the experimentally observed event plane correlators in terms of linear response to the corresponding participant plane correlators,

except for one event plane correlator: $\langle \cos(2\Psi_2 - 6\Psi_3 + 4\Psi_4) \rangle$ [3, 24]. Figure 6 shows that we agree with their findings. Like them, we do not have an explanation for the apparent non-linearity of the response leading to the 2-3-4 flow correlator.

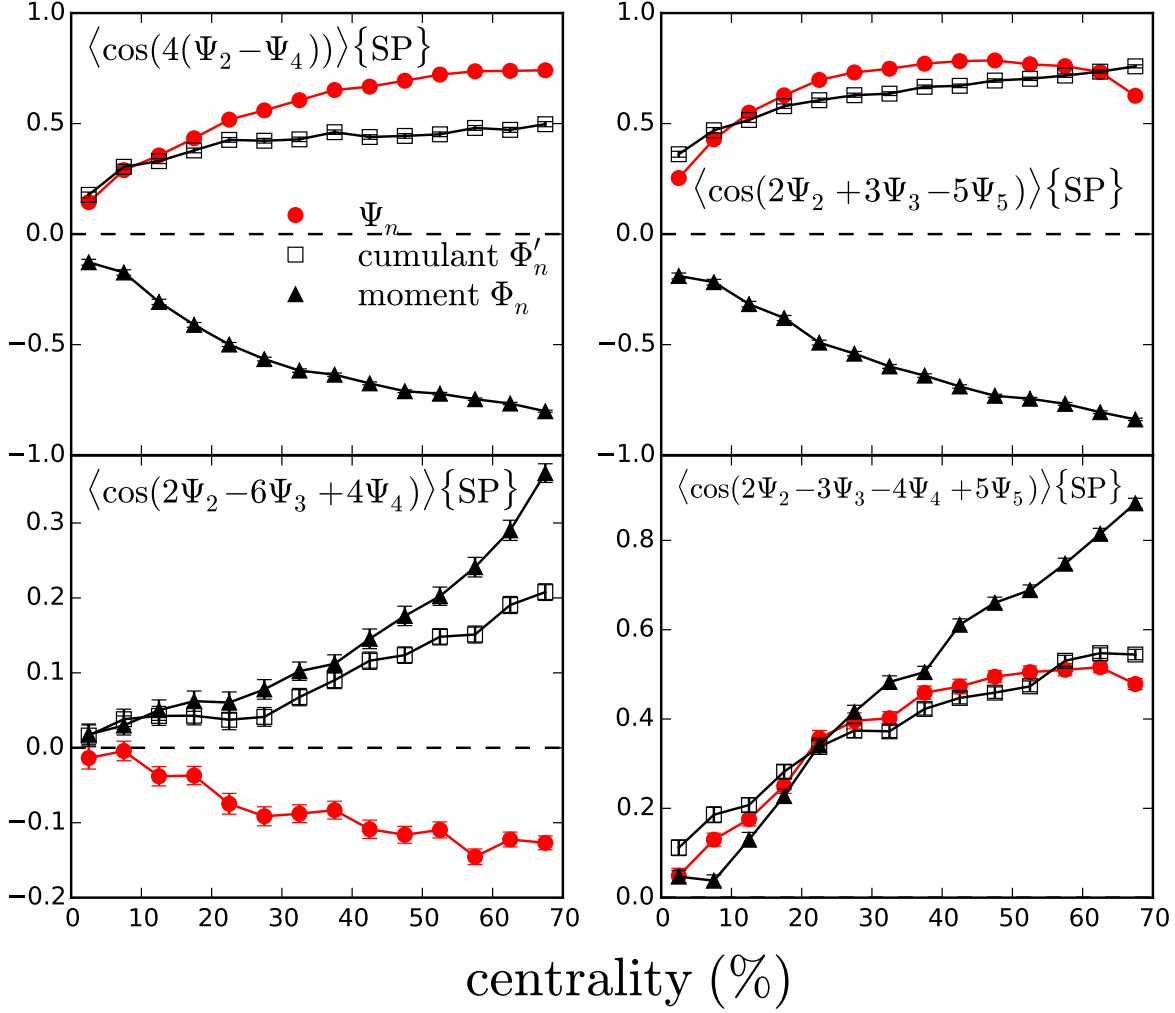


FIG. 6. (Color online) Event plane correlations and the corresponding participant plane correlations from viscous hydrodynamics with MC-Glauber initial conditions and $\eta/s = 0.08$. 42000 minimum bias (0-70% centrality) events are cut into 14 equal centrality classes according to their multiplicity. Red circles represent event plane correlations between flow vectors integrated over the p_T range $p_T \in [0.3, 3.5)$ GeV/c, black triangles represent the corresponding participant plane correlators with moment-defined eccentricities while black hollow squares represent the corresponding participant plane correlators of the cumulant-defined eccentricity vectors.

To further examine the (non-)linearity of the hydrodynamic response, we use the ratio between flow and eccentricity as a function of eccentricity. Since in Eqs. (9) the square of the magnitude of the linear response term is averaged over events, we use the root mean square

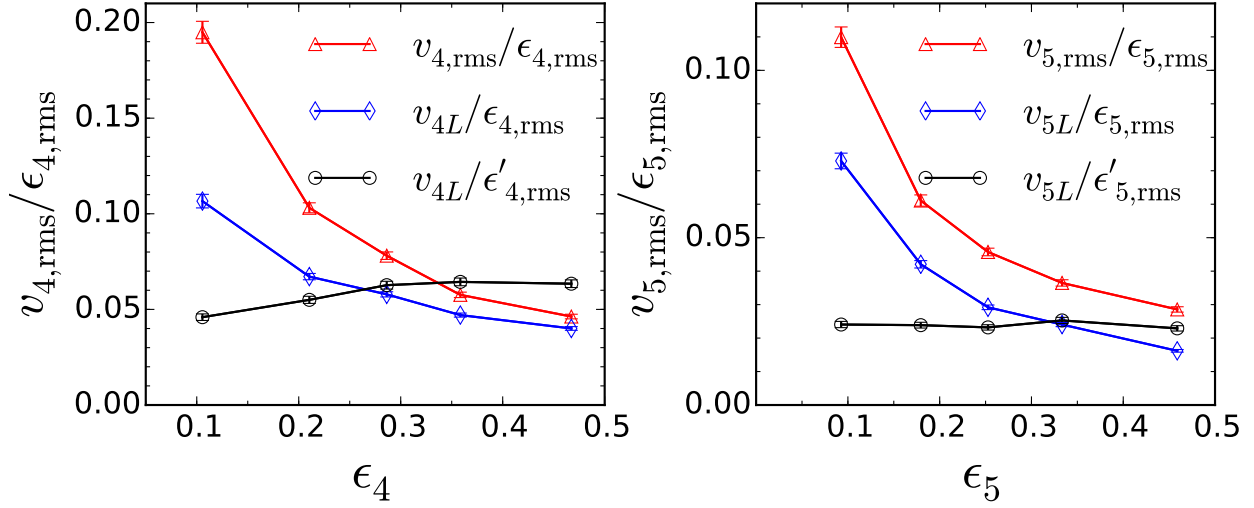


FIG. 7. (Color online) Check of the linearity between v_n and ϵ_n , using 2000 ideal hydrodynamic events at 40-50% centrality. Red triangles represent $v_n\{2\}/\epsilon_n\{2\}$, blue diamonds represent $v_{nL}/\epsilon_n\{2\}$ and black circles are $v_{nL}/\epsilon'_n\{2\}$. The left panel is for $n = 4$ while the right panel is for $n = 5$.

eccentricities for normalization:

$$\begin{aligned}
 v_{n,\text{rms}} &= \sqrt{\langle v_n^2 \rangle}, \\
 \epsilon_{n,\text{rms}} &= \sqrt{\langle |\mathcal{E}_n|^2 \rangle}, \\
 \epsilon'_{n,\text{rms}} &= \sqrt{\langle |\mathcal{E}'_n|^2 \rangle},
 \end{aligned} \tag{A2}$$

with \mathcal{E}'_n from Eqs. (A1). In Fig. 7 we plot the ratios v_n/ϵ_n as functions of ϵ_n for different definitions of numerator and denominator as described in the legend, for $n = 4$ and 5, using 2000 ideal hydrodynamic events at 40-50% centrality. We find that, different from $v_n\{2\}/\epsilon_n\{2\}$ (shown as red triangles) and $v_{nL}/\epsilon_n\{2\}$ (shown as blue diamonds), $v_{nL}/\epsilon'_n\{2\}$ (shown as black circles) is almost independent of the ϵ_n used in the denominator, suggesting that V_{nL} is indeed the linear response to \mathcal{E}'_n .

-
- [1] U. Heinz and R. Snellings, Ann. Rev. Nucl. Part. Sci. **63**, 123 (2013).
 - [2] D. Teaney and L. Yan, Phys. Rev. C **83**, 064904 (2011).
 - [3] D. Teaney and L. Yan, Nucl. Phys. A **904-905**, 365c (2013).
 - [4] J. Jia and S. Mohapatra, Eur. Phys. J. C **73**, 2510 (2013).
 - [5] J. Jia and D. Teaney, Eur. Phys. J. C **73**, 2558 (2013).

- [6] G. Aad *et al.* [ATLAS Collaboration], Phys. Rev. C **90**, no. 2, 024905 (2014).
- [7] Z. Qiu and U. Heinz, Phys. Lett. B **717**, 261 (2012).
- [8] G. Aad *et al.* [ATLAS Collaboration], Phys. Rev. C **92**, no. 3, 034903 (2015).
- [9] J. Qian and U. Heinz, Phys. Rev. C **94**, 024910 (2016).
- [10] J. Adam *et al.* [ALICE Collaboration], Phys. Rev. Lett. **117**, 182301 (2016).
- [11] L. Yan and J. Y. Ollitrault, Phys. Lett. B **744**, 82 (2015).
- [12] J. Qian, U. Heinz and J. Liu, Phys. Rev. C **93**, 064901 (2016).
- [13] H. Song and U. Heinz, Phys. Lett. B **658**, 279 (2008); Phys. Rev. C **77**, 064901 (2008); and Phys. Rev. C **78**, 024902 (2008).
- [14] C. Shen, Z. Qiu, H. Song, J. Bernhard, S. Bass and U. Heinz, Comput. Phys. Commun. **199**, 61 (2016).
- [15] R. S. Bhalerao, J. Y. Ollitrault and S. Pal, Phys. Rev. C **88**, 024909 (2013).
- [16] B. Betz, M. Gyulassy, M. Luzum, J. Noronha, J. Noronha-Hostler, I. Portillo and C. Ratti, arXiv:1609.05171 [nucl-th].
- [17] U. Heinz, Z. Qiu and C. Shen, Phys. Rev. C **87**, no. 3, 034913 (2013).
- [18] P. Di Francesco, M. Guillebaud, M. Luzum and J. Y. Ollitrault, arXiv:1612.05634 [nucl-th].
- [19] J. Jia, J. Phys. G **41**, 124003 (2014).
- [20] X. Zhu, Y. Zhou, H. Xu and H. Song, arXiv:1608.05305 [nucl-th].
- [21] H. Niemi, G. S. Denicol, H. Holopainen and P. Huovinen, Phys. Rev. C **87**, 054901 (2013).
- [22] D. Teaney and L. Yan, Phys. Rev. C **86**, 044908 (2012).
- [23] D. Teaney and L. Yan, Phys. Rev. C **90**, 024902 (2014).
- [24] D. Teaney and L. Yan, J. Phys. Conf. Ser. **446**, 012026 (2013).
- [25] Ohio Supercomputer Center (1987), <http://osc.edu/ark:/19495/f5s1ph73>.